gebiology

Geobiology (2014), **12**, 557–574 DOI: 10.1111/gbi.12113

Spatial variability in photosynthetic and heterotrophic activity drives localized $\delta^{13}C_{org}$ fluctuations and carbonate precipitation in hypersaline microbial mats

J. HOUGHTON,[1] D. FIKE,[1] G. DRUSCHEL,[2] V. ORPHAN,[3] T. M. HOEHLER[4] AND D. J. DES MARAIS[4]

[1]*Department of Earth and Planetary Sciences, Washington University, St. Louis, MO, USA*
[2]*Department of Earth Sciences, Indiana University-Purdue University Indianapolis, Indianapolis, IN, USA*
[3]*Division of Geological and Planetary Sciences, California Institute of Technology, Pasadena, CA, USA*
[4]*Exobiology Branch, NASA Ames Research Center, Moffett Field, CA, USA*

ABSTRACT

Modern laminated photosynthetic microbial mats are ideal environments to study how microbial activity creates and modifies carbon and sulfur isotopic signatures prior to lithification. Laminated microbial mats from a hypersaline lagoon (Guerrero Negro, Baja California, Mexico) maintained in a flume in a greenhouse at NASA Ames Research Center were sampled for $\delta^{13}C$ of organic material and carbonate to assess the impact of carbon fixation (e.g., photosynthesis) and decomposition (e.g., bacterial respiration) on $\delta^{13}C$ signatures. In the photic zone, the $\delta^{13}C_{org}$ signature records a complex relationship between the activities of cyanobacteria under variable conditions of CO_2 limitation with a significant contribution from green sulfur bacteria using the reductive TCA cycle for carbon fixation. Carbonate is present in some layers of the mat, associated with high concentrations of bacteriochlorophyll *e* (characteristic of green sulfur bacteria) and exhibits $\delta^{13}C$ signatures similar to DIC in the overlying water column (−2.0‰), with small but variable decreases consistent with localized heterotrophic activity from sulfate-reducing bacteria (SRB). Model results indicate respiration rates in the upper 12 mm of the mat alter *in situ* pH and HCO_3^- concentrations to create both phototrophic CO_2 limitation and carbonate supersaturation, leading to local precipitation of carbonate minerals. The measured activity of SRB with depth suggests they variably contribute to decomposition in the mat dependent on organic substrate concentrations. Millimeter-scale variability in the $\delta^{13}C_{org}$ signature beneath the photic zone in the mat is a result of shifting dominance between cyanobacteria and green sulfur bacteria with the aggregate signature overprinted by heterotrophic reworking by SRB and methanogens. These observations highlight the impact of sedimentary microbial processes on $\delta^{13}C_{org}$ signatures; these processes need to be considered when attempting to relate observed isotopic signatures in ancient sedimentary strata to conditions in the overlying water column at the time of deposition and associated inferences about carbon cycling.

Received 18 March 2014; accepted 30 August 2014

Corresponding author: J. Houghton. Tel.: +1 314 935 5610; fax: +1 314 935 7361; e-mail: jhoughton@levee.wustl.edu

INTRODUCTION

The carbon isotopic compositions preserved in marine sediments provide a record of global carbon cycling that can be impacted and variably overprinted by several factors including climate, heterogeneity within basins, biological processes within the sediments prior to lithification, and diagenetic processes after lithification (Kump & Arthur, 1999; Orphan *et al.*, 2001; Swart, 2008; Grotzinger *et al.*, 2011). Frequently, stratigraphic records of $\delta^{13}C_{carb}$ in primary carbonates are interpreted as a function of changes in marine dissolved inorganic carbon (DIC) that reflects changes in basin-wide biological processes (Kump & Arthur, 1999; Grotzinger *et al.*, 2011; Saltzman & Tho-

© 2014 John Wiley & Sons Ltd

mas, 2012). However, microbial activity could alter local $\delta^{13}C_{DIC}$, overprinting the signature from the water column in carbonates precipitated within the sediments (Dupraz & Visscher, 2005; Schrag *et al.*, 2013). Likewise, the $\delta^{13}C$ of organic carbon preserved in sediments represents the cumulative effects of microbial primary production and heterotrophic reprocessing in the sediments that may overprint the isotopic composition associated with primary water column activity. Further, $\delta^{13}C_{org}$ values reflect not just water column processes, but also integrate ongoing microbial activity during deposition and lithification. Microbial mats, both lithifying and non-lithifying, represent an endmember system in which microbial activity could affect the $\delta^{13}C$ signature of DIC and associated carbonates. Precambrian stromatolites from shallow marine environments are thought to represent the earliest photosynthetic lithifying microbial consortia that significantly impacted ocean and atmospheric chemistry (Holland *et al.*, 1994; Hoehler *et al.*, 2001), while simultaneously leaving a record of their presence in the form of carbonate structures preserved in the rock record (Grotzinger & Knoll, 1999; Riding, 2000). Following the Precambrian, when stromatolite formation became more limited, mat-forming microbial consortia remained important drivers of biogeochemical change in confined basins, shallow lagoon, and reef settings, responsible for lithification of carbonate material, decreasing erosion rates, and regulating global carbon cycling (Dupraz & Visscher, 2005). Modern laminated microbial mats found today are analogues for biogenic processes similar to those that formed ancient stromatolites now preserved in the rock record (Des Marais *et al.*, 1992).

Microbial mats in hypersaline lagoons such as those at Guerrero Negro, Baja California Sur, Mexico, are ideal analogues to study microbial sulfur and carbon cycling responsible for formation of stable isotope signatures in the absence of other forcing factors, being nearly self-contained ecosystems with minimal grazing or bioturbation to disturb the laminated signatures (Jørgensen *et al.*, 1979; Des Marais *et al.*, 1989). The fine-scale laminations in these mats are remnants of spatial heterogeneity in the depositional environment allowing colonization of different functional groups of photosynthetic micro-organisms within the ecosystem (Farmer & Des Marais, 1994), each specialized for a different role in the carbon and sulfur cycle (Fig. 1). The microbial mats at Guerrero Negro are dominated by cyanobacteria (CYA) *Microcoleus chthonoplastes* in the oxic portions of the photic zone (Canfield & Des Marais, 1993; Ley *et al.*, 2006) with possibly greater abundances (but less biomass) of filamentous anoxygenic phototrophs (FAP) such as *Chloroflexus and Chlorothrix* sp. (Harris *et al.*, 2013; Ley *et al.*, 2006). Also present in abundance are green sulfur bacteria (GSB) in the *Chlorobium* genus, purple sulfur bacteria of the *Chromatium* genus, and colorless sulfur bacteria (CSB) such as *Beggiatoa* sp. (Jorgensen & Des Marais, 1986a; Canfield & Des Marais, 1993; Dillon *et al.*, 2009; Harris *et al.*, 2013). The ecological organization of these clades is complex. Briefly, cyanobacteria (CYA) and other phototrophs produce organic carbon compounds, which are then partially or completely oxidized by, among others, aerobic heterotrophs and sulfate-reducing bacteria (SRB), which produce sulfide in turn. Microbially produced sulfide is then utilized by phototrophic purple sulfur bacteria (PSB) and autotrophic colorless sulfur bacteria (CSB), using either external or internal CO_2 (aq) and organic compounds, respectively (Fig. 1). CO_2 (aq) produced during decomposition, if not consumed *in situ*, would alter the abundance and isotopic composition of the local DIC pool and possibly impact carbonate formation at depth, depending on the pH and saturation of calcite. Production of alkalinity during respiration, particularly resulting from the activity of SRB (Bosak & Newman, 2005), may therefore alter the carbon isotope signature of carbonate precipitated *in situ* during microbial mat formation.

Studies of sulfate-reducing bacteria within the Guerrero Negro mats revealed high biodiversity of SRB (Frund & Cohen, 1992; Teske *et al.*, 1998; Minz *et al.*, 1999). Elevated sulfate reduction rates are co-located with higher O_2 production rates from cyanobacterial photosynthesis in the oxic surface layers that exceed rates measured in the anoxic layers at depth (Canfield & Des Marais, 1991). Sulfate reduction therefore could produce considerable concentrations of alkalinity and hence bicarbonate within the uppermost layers of the mat. The diel cycling of O_2 (aq) and H_2S (aq) as functions of light intensity has been studied in detail, revealing shifting chemoclines (Jørgensen *et al.*, 1979; Bebout *et al.*, 2002) leading to migrating microbial populations from various functional groups (Jorgensen &

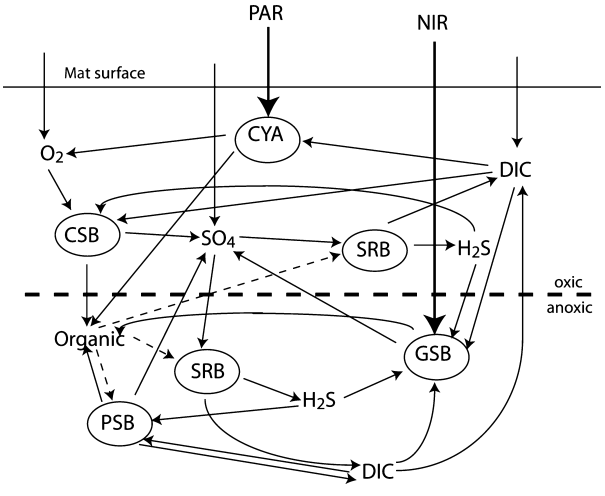

Fig. 1 Generalized schematic of carbon and sulfur cycling within the Guerrero Negro microbial mats. Complex relationships exist between different functional guilds, with recycling of biogenic products common. Dashed arrows indicate decomposition processes.

© 2014 John Wiley & Sons Ltd

Des Marais, 1986b; Garcia-Pichel *et al.*, 1994; Bebout & Garcia-Pichel, 1995; Teske *et al.*, 1998), and opportunistic changes in metabolic functions by both phototrophs and chemoautotrophs (Jorgensen & Des Marais, 1986b; de Wit & van Gemerden, 1990). During the day, photosynthesis drives O_2 (aq) concentrations very high, restricting measurable H_2S (aq) to deeper within the mat, while at night, the chemocline rises close to the mat surface and H_2S (aq) can accumulate in the overlying water column (Jørgensen *et al.*, 1979; Fike *et al.*, 2009).

Stable isotopes of aqueous sulfur compounds within laminated hypersaline mats indicate variable fractionation effects between SO_4 and H_2S at very fine scales that could be functions of sulfate reduction rates, electron donor source, or physical variability affecting diffusivity within the mat (Fike *et al.*, 2008, 2009). The first two possible explanations are directly connected to carbon cycling within the mat and are likely the most important processes that impact the sulfur isotopic composition. Stable carbon isotopes of organic material and DIC have been analyzed at cm-scale resolution in the Guerrero Negro mats previously and indicate heavier than expected $\delta^{13}C$ values for organic mat material (Des Marais *et al.*, 1989; Kelley *et al.*, 2006). The current model to explain the observed $\delta^{13}C$ of mat material invokes limited CO_2 concentrations available to phototrophs (Des Marais *et al.*, 1989), assuming that activity of these organisms dictates the baseline isotopic signature of the mat (i.e., active, relict, and heterotrophically reprocessed photosynthetic biomass constitutes the bulk of the organics in the mat). Here, we present co-registered $\delta^{13}C_{org}/\delta^{13}C_{carb}$/carbonate abundance/pigment profiles at 1-mm resolution within laminated microbial mats to investigate the relative impact of metabolic clades on these signals. These results are interpreted using a simple flux model that accounts for carbon fractionation by all functional groups in the mat, including phototrophs and heterotrophs. Isotopically labeled amendment experiments designed to stimulate sulfate reduction are used to constrain the impact and spatial location of decomposition in the model. The model also predicts the stimulation of carbonate precipitation by sulfate-reducing bacteria.

METHODS

Field site

Laminated microbial mat from Guerrero Negro, Baja California Sur, Mexico Pond 4 near 5 was collected in September 2010 and maintained in a flume at the NASA Ames rooftop greenhouse 'collaboratory' illuminated by natural light (Bebout *et al.*, 2002). The recirculated water in the flume has a salinity 2.5 times that of seawater, designed to be similar to the *in situ* composition found in the hypersaline lagoon.

Sampling

Mat material was cored with plastic straws (6 mm diameter) and frozen at −80 °C for isotopic analysis. Representative night and day cores of unaltered flume mat were collected in December of 2011 just prior to sunrise (4:40 AM) and after (8:20 AM), respectively. Larger samples of mat material for incubation experiments were obtained by coring with a cutoff 60-mL syringe (25 mm diameter). Incubations were conducted in 100-mL screw cap bottles using flume water under ambient lighting conditions in the greenhouse. Acetate enrichment incubations were in flume water amended with 250 μM ^{13}C-acetate and 500 μM ^{15}N-NH_3.

Vertical electrochemical profiling was carried out to determine the redox reactive chemical species through the overlying water and into the mats. A glass Au–Hg amalgam microelectrode was lowered at 1000-m increments vertically through the mat using a micromanipulator. The electrodes were constructed in the laboratory according to methods published in Brendel & Luther (1995). A sequence of ten cyclic voltammograms (−0.1 to −1.8 V vs. Ag/AgCl at 1 V s^{-1} with 2 s deposition at −0.1 V) was obtained from each electrode at each depth using DLK-60 (AIS Instruments, Ringoes, NJ, USA) software. The current response of the last five scans of each sequence of 10 was measured and then averaged for each depth where voltammograms were obtained (DLK-60 Analysis program; AIS Instruments). The variability between scans within one sequence is extremely small (typically <1%). The electrodes were calibrated using 2-point O_2 calibrations (air-saturated, assuming saturation = 262 μM for 1 M $MgCl_2$ at 15 °C after Millero *et al.* (2002) and N_2 purged where O_2 is 0 μM) and standard additions of $MnCl_2$ standards to N_2 purged water. Calibration for other ions has been performed relative to Mn^{2+}, with oxygen peaks at −1.3 and −0.3 V (O_2 and H_2O_2), Mn(II) at −1.6 V, Fe(II) at −1.4 V, Fe(III) at −0.6 V, H_2S/HS^- at −0.8 V, and $S_2O_3^{2-}$ at −0.2 V. These ions can be calibrated for any electrode using the pilot ion method (Meites & Delahey, 1966; Brendel & Luther, 1995; Slowey & DiPasquale, 2012).

Isotopic analyses

Frozen core samples were sliced at 1-mm intervals, dried, and crushed for bulk mat, organic carbon, and carbonate $\delta^{13}C$ analysis. For carbonate $\delta^{13}C$, dried bulk mat material was reacted for 4 h at 70 °C with an excess of 100% H_3PO_4 in He-flushed, sealed tubes. Evolved CO_2 was sampled with a Thermo Finnigan Gas Bench II (Thermo, Bremen, Germany), and isotopic ratios were measured with a Thermo Delta V Advantage. Isotopic measurements were calibrated against 3 in-house standards that have been calibrated against international standards NBS-18, NBS-19, and LSVEC, with analytical errors of <0.1‰ (1σ) for

© 2014 John Wiley & Sons Ltd

$\delta^{13}C_{carb}$. Both bulk mat samples and mat organic carbon $\delta^{13}C$ were analyzed on a Costech ECS 4010 Elemental Analyzer (Valencia, CA, USA) connected to a Thermo Delta V Plus isotope ratio mass spectrometer. Dried and crushed mat material was directly analyzed for bulk mat carbon isotopic signature (i.e., bulk carbon $\delta^{13}C$ values were mixtures of carbonate and organic carbon). To isolate the organic carbon signature, mat was sliced and acidified with dilute HCl (pH ~1.5) either wet or dry and then rinsed three times to remove excess acid prior to drying. The mass of dried mat material combusted was varied for each sample to give a constant peak size for CO_2 on the mass spectrometer. Isotopic measurements were calibrated against NBS-21 graphite, IAEA-C6 sucrose, and IAEA-CH3 cellulose standards. All samples were measured in duplicate with a reproducibility of <0.2‰ (1σ). Carbon isotope compositions are expressed in standard δ-notation as ‰-deviations from V-PDB:

$$\delta^{13}C = \left\{ \frac{\left(^{13}C/^{12}C\right)_{sample}}{\left(^{13}C/^{12}C\right)_{std}} - 1 \right\} \times 10^3 \quad (1)$$

For the purposes of this paper, fractionation factors from the literature between a reactant (R) and product (P) are used as follows:

$$\varepsilon_{R\text{-}P} \cong \Delta_{R\text{-}P} = \delta^{13}C_R - \delta^{13}C_P \quad (2)$$

Pigment analyses

A replicate frozen core sample was sliced at 1-mm intervals and processed to determine pigment abundance by dissolving in 2 mL of 7:2 acetone:methanol for 30 min at 4 °C in the dark (Frigaard *et al.*, 1996). The samples were centrifuged, and the supernatant analyzed spectrophotometrically on a Thermo Evolution 60 UV-VIS spectrophotometer (Thermo). Scans from 200–1200 nm were performed and analyzed using linear combination analysis in the SIXPACK software (Webb, 2005). Reference scans for common pigments (chlorophyll *a*, *b*; bacteriochlorophyll *a*, *b*, *c*, *d*, *e*) were obtained from Frigaard *et al.* (1996).

Modeling

The processes of DIC transport within microbial mats are represented by the following simplified equation:

$$DIC_{out} \underset{flux_{out}}{\overset{flux_{in}}{\longleftrightarrow}} DIC_{mat} \xrightarrow{flux_{fix}} C_{org} \quad (3)$$

where the $flux_{out} = flux_{in} - flux_{fix}$ and the fixation flux ($flux_{fix}$) is due to primary production only. The $\delta^{13}C$ of bioavailable CO_2 (aq) (−7.3‰) is derived from the conversion of CO_2 (g) with a $\delta^{13}C$ of −8.35‰ at Baja (Keeling *et al.*, 2008) with an equilibrium ε of −1.09‰ upon conversion to CO_2 (aq). Bicarbonate in equilibrium with dissolved CO_2 (g) has a $\delta^{13}C$ of −1.0‰ ($\varepsilon_{CO2(g)\text{-}HCO3-} = -7.4$; Mook *et al.*, 1974), and the equilibrium $\varepsilon_{HCO3\text{-}CaCO3(s)}$ is +1.77‰ (Emrich *et al.*, 1970). The isotopic signature of the mat material is a function of the composition of CO_2 (aq), sourced from the overlying water column in equilibrium with atmospheric CO_2, offset by isotopic fractionation during net microbial activity:

$$\delta^{13}C_{org} = \delta^{13}C_{CO2(aq)} - \Delta_{micr} \quad (4)$$

Here, Δ_{micr} reflects the weighted average of isotopic fractionation for various carbon fixation pathways. Because these pathways often have diagnostic pigment distributions, the relative abundances of pigments can be used to approximate Δ_{micr} in the mat due to primary production as follows:

$$\Delta_{micr} = (f_{CYA} \cdot \varepsilon_{CYA} + f_{PSB} \cdot \varepsilon_{PSB} + f_{GSB} \cdot \varepsilon_{GSB}) \quad (5)$$

where the fraction of cyanobacteria (f_{CYA}) is equal to that of chlorophyll *a*, the fraction of purple sulfur bacteria (f_{PSB}) and purple non-sulfur bacteria were approximated by the sum of bacteriochlorophyll *a* and *b*, and the fraction of green sulfur bacteria (f_{GSB}) is equal to bacteriochlorophyll *e*. The bchla content of GSB is negligible compared to the bchle content (Overmann *et al.*, 1992), and thus, the abundance of bchla in the mat is considered here to represent only the PSB and PnonSB clades. The dominant pigments of purple non-sulfur bacteria are indistinguishable from those of PSB (Table 1). As both groups also use the Calvin Benson cycle to fix carbon, and thus have similar fractionation factors, this does not impact our analysis. For our purposes here, we treat each 1-mm layer of the mat as a separate box model calculated using equations (4) and (5) with fractionation factors for all groups of primary producers reported in Table 1.

We tested the model accounting for limiting DIC outlined in Des Marais *et al.* (1989) by modifying the fractionation factor from equation (5) as follows:

$$\Delta_{overall} \approx \frac{DIC_{flux_{out}}}{DIC_{flux_{out}} + DIC_{flux_{fixed}}} \times \Delta_{micr} \quad (6)$$

where the ratio of DIC $flux_{out}$/(DIC $flux_{out}$ + DIC $flux_{fixed}$), hereafter referred to as the carbon fixation factor (f_{fix}), is a function of diffusivity within the mat and the balance between carbon fixation and respiration in the photic zone. The carbon fixation factor (f_{fix}) acts to decrease isotopic fractionation during carbon fixation when very high microbial activity creates limitation in the supply

© 2014 John Wiley & Sons Ltd

© 2014 John Wiley & Sons Ltd

Table 1 Characteristics of clades found in photosynthetic microbial mats

Group	Genus	chla	chlb	bchla	bchlb	bchlc	bchld	bchle	O_2 tolerance	C source	S utilization	ε C (‰)
FAP	*Oscillochloris*			x		x	x		Fac. aerobe	Organics preferred (some use Calvin cycle)	Photoautotrophic growth on H_2S to S (4)	
ABC	*Acidiphilium*			(x)					Aerobic	Organics	Non-photosynthetic sulfur oxidation (H_2S, S_2O_3, SO_3, S) to SO_4 (4)	
GSB	*Chlorobium*			x		x	x	x	Strict anaerobe	CO_2 (reductive TCA)	Obligately phototrophic growth on H_2S, S, S_2O_3, S_4O_6 to SO_4 (4)	(1) 4 to 13; (3) **18** to 20
PnonSB	Varied within α- and β-proteobacteria			x	x				fac. anaerobe	Photoheterotrophic growth (5)	Photoheterotrophic/ photoautotrophic/ chemoorganotrophic growth using varied sulfur compounds (4)	
PSB	Chromatiaceae			x	x				Strict anaerobe	Photoorganoheterotrophic growth using organics (4) (Calvin cycle)	Photoautotrophic growth on H_2S, S, S_2O_3, SO_3	(2) **33.7** to 18.3
PSB	Ectothiorhodo-spiraceae			x	x				Anaerobic	HCO_3 or organics (Calvin cycle)	Photoheterotrophic or photoautotrophic growth on H_2S to polysulfides (4)	(3) 15 to **34** (27)
CYA		x								CO_2 (Calvin Benson)		(6) 22 to **26**

FAP, filamentous anoxygenic phototrophs; ABC, aerobic phototrophs; GSB, green sulfur bacteria; PnonSB, purple non-sulfur bacteria; PSB, purple sulfur bacteria; GnonSB, green non-sulfur bacteria; CYA, cyanobacteria.(1) from Hayes (2001); (2) from Wong *et al.* (1975); (3) from Zyakun *et al.* (2009); (4) Dahl (2008); (5) Sander & Dahl (2008); and (6) Sumner (2001). Bold values were used in the model described in the text.

of CO_2 to the cells. We have also tested a modified version of equation (6) that allows separate carbon fixation factors modifying cyanobacteria fractionation (Δ_{CYA}) and fractionation by the photosynthetic sulfur bacteria ($\Delta_{P/GSB}$) and includes an additional factor for decomposition (Δ_{decomp}) that alters the isotopic composition from primary productivity values. This is motivated by the often close association between PSB/GSB and SRB (based on the respective consumption and production of HS^-), which would allow a tight recycling of carbon and sulfur within the mat, thereby making PSB/GSB less dependent on diffusion (or *in situ* respeciation from bicarbonate) of CO_2 (aq) from the water column (Fig. 1). Therefore, the flux ratio for CYA can be different from the flux factor for PSB + GSB, giving a modified equation from (6) as:

$$\Delta_{overall} \approx (f_{fix})_{CYA} \cdot (\Delta_{micr})_{CYA} + (f_{fix})_{P/GSB} \cdot (\Delta_{micr})_{P/GSB} + \Delta_{decomp} \quad (7)$$

Thus, Δ_{CYA} and $\Delta_{P/GSB}$ are functions of primary productivity, and Δ_{decomp} is a function of secondary decomposition processes at depth in the mat, indicated by dashed lines in Fig. 1.

A separate speciation model was constructed to resolve the influence of diffusion, respiration, and carbon fixation on total DIC concentrations, bioavailable CO_2 (aq), and carbonate saturation with depth in the mat. The model first speciates inorganic carbon using total DIC concentration and pH in the overlying water column. Then, by setting the diffusivity, respiration rate, and fixation rate at 1-mm intervals, concentrations of CO_2 (aq), HCO_3^- , and CO_3^- are calculated and summed to total DIC:

$$\frac{\partial C}{\partial t} = D\frac{\partial^2 C}{\partial x^2} + R_{net} \quad (8)$$

where R_{net} is the net reaction rate and equals the respiration rate (R_{resp}) minus the fixation rate (R_{fix}) in units of moles per litre. The concentration gradient is described by:

$$\frac{\partial^2 C}{\partial x^2} = \frac{C_{i+1} + 2C_i + C_{i-1}}{\Delta x^2} \quad (9)$$

where C is the concentration of total DIC in moles per litre and Δx is 1 mm. The concentrations of CO_2 (aq), HCO_3^-, and $S_2O_3^{2-}$ are adjusted by varying respiration and fixation rates at each depth until a steady state (determined using an iterative solver) is reached that matches the observed total DIC concentrations reported for Guerrero Negro mats in Kelley *et al.* (2006). For our purposes, diffusivity is assumed to be constant with depth in the mat at 10^{-5} cm^2 s^{-1} (Bebout *et al.*, 2002; and references therein). The balance between carbon fixation and CO_2 availability is subject to respeciation and diffusion rates in the mat. In the photic zone (top 3 mm), the rate of CO_2 fixation is greater than diffusion of CO_2, resulting in CO_2 limitation and requiring that modeled inorganic carbon be respeciated at each depth using the pH profile measured in this study. Calcite saturation is calculated as Q/K, where K, calculated using the equation of Millero (1995) for 27 °C and a salinity of 85 ppt, is $2.32e^{-6}$, and $[Ca^{++}]$ is assumed to be 25 mM at all depths.

RESULTS

Isotopic analysis of primary mat

The microbial mat growing in the greenhouse at Ames is laminated, with clearly visible layering of pigmented photosynthetic primary producers (Fig. 2). After slicing and drying bulk mat material, the powdered solid also retains layering within the shades of brown, ranging from greenish to pinkish/orange. Although the visible pigment layering in the wet mat is quite fine (sub-mm), the mat was sliced every 1 mm to obtain enough solid material for isotopic analyses. The $\delta^{13}C$ signature with depth in the bulk mat material ranges from −7.7‰ to −15.1‰, with oscillations that alternate with the coloration of the dried mat material (Fig. 3), suggesting a link between the isotopic signature and the abundances of active/relict primary producers within each layer. In addition, mm-scale variability is fairly consistent over lateral distances of several cm as well as throughout the diel cycle, with no significant difference in isotopic composition or color of mat material between samples taken in full sun (8:20 AM) vs. just prior to sunrise (4:40 AM) (Fig. 3).

Variable amounts of carbonate were found throughout the mat material at the 1-mm scale. Spherical carbonate grains ranged in size from 20 to 260 μm, predominantly found in GSB-rich layers. The size and shape of these carbonate grains are consistent with previously reported carbonate formed in situ within degraded mat layers associated with heterotrophs and PSB (Kuhl *et al.*, 2003). Mat samples were analyzed for carbonate percent and $\delta^{13}C_{carb}$ prior to acidification of the remaining material for analysis of organic $\delta^{13}C$. The amount of carbonate ranged from 0 to 55% of mass in each layer, with most layers containing <10% (Fig. 4), consistent with the distribution of white carbonate nodules in the mat shown in Fig. 2C. Organic carbon $\delta^{13}C$ was less variable than the bulk mat $\delta^{13}C$, ranging from −9.7‰ to −12.9‰ (Fig. 4), indicating that the bulk $\delta^{13}C$ variability was driven by variable amounts of carbonate. The percent carbonate data show a weak correlation with bchle ($r = -0.14$) (Fig. 5), and therefore, carbonate precipitation may be related to the specific community composition, in particular the abundance of (bchle-containing) green sulfur bacteria in each layer (Dahl *et al.*, 2008; Zyakun *et al.*, 2009). The carbon-

© 2014 John Wiley & Sons Ltd

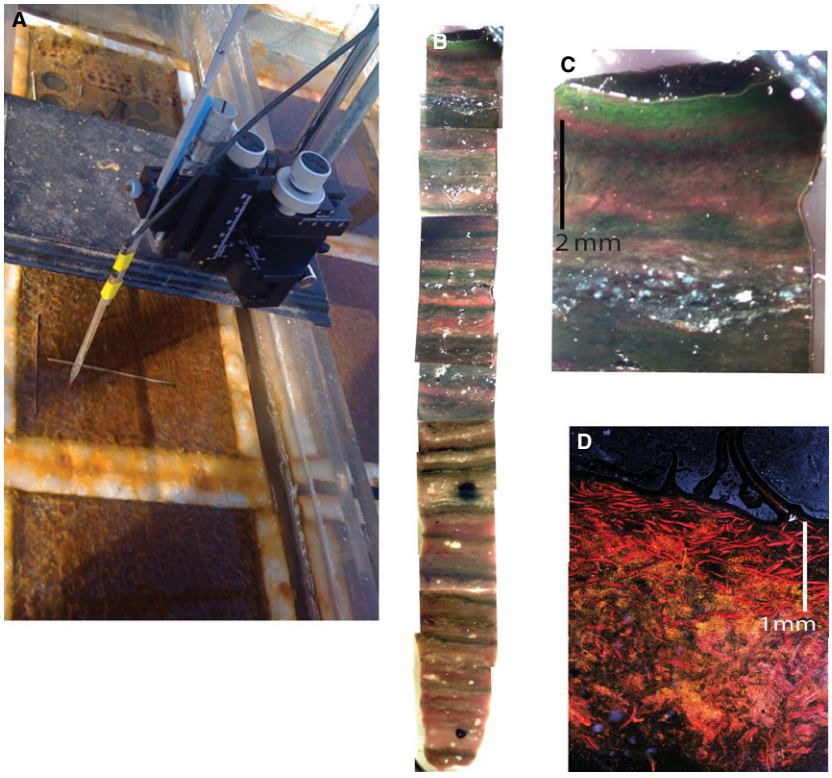

Fig. 2 (A) Profiling through the mat in the greenhouse at Ames. Configuration of the flume with mat pieces is described in Bebout *et al.* (2002). (B) Cores of mat were taken using plastic straws and frozen in liquid nitrogen immediately. This core is 4 cm long and was used for pigment analysis described below. (C) Close-up view of the top of the mat showing the complexity of interlaced cyanobacteria (bright green), purple sulfur bacteria (purple), and green sulfur bacteria (blueish green). The interspersed white material is carbonate within the mat at ~4 mm depth. (D) Close-up view of autofluorescence in the top of the mat [top half of (C)] in false color. Taken on a Leica S8APO confocal microscope with 3 channels: 620–710 nm (red; chla marking CYA), 550–570 nm (green; isorenieratene marking GSB + PSB), and 450–480 nm (blue; beta-carotene marking FAP).

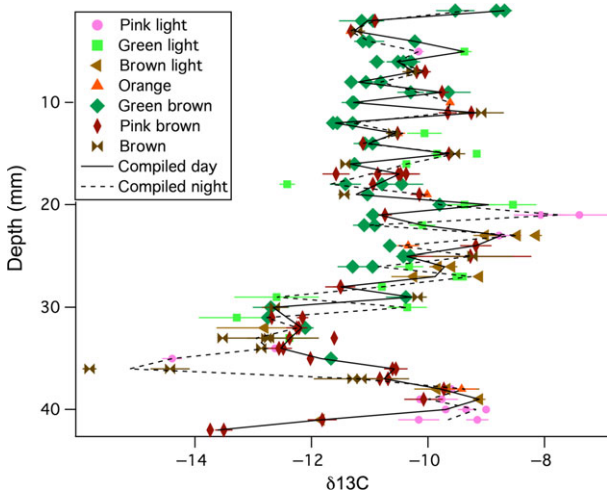

Fig. 3 Comparison of $\delta^{13}C$ signature of bulk mat material taken just before dawn (dashed line) and at peak sun (solid line). Colored symbols represent shades of color of the dried crushed mat material at the time of analysis. Cores of mat were taken several cm apart.

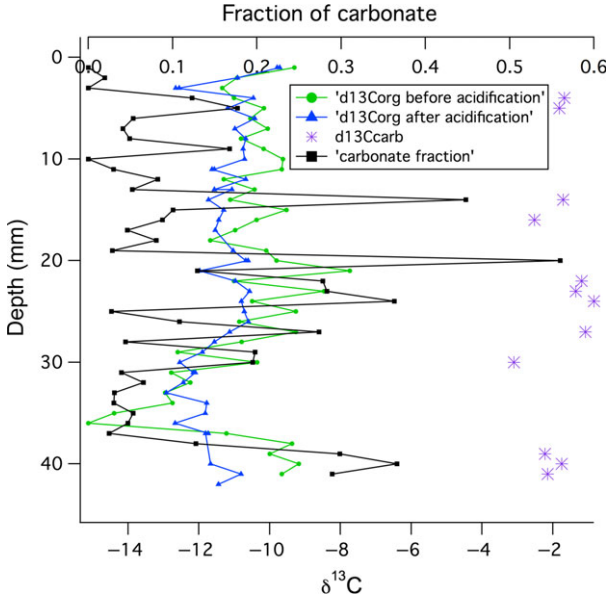

Fig. 4 Measured profiles of bulk mat $\delta^{13}C$ (green circles), organic carbon $\delta^{13}C$ (blue triangles), and carbonate $\delta^{13}C$ (purple stars). The carbonate $\delta^{13}C$ values were measured for all samples with enough remaining material. The measured abundance of carbonate shown in % (black squares) was estimated by calibrating the peak area on the Gas Bench-Delta V using carbonate standards.

ate $\delta^{13}C$ is fairly constant over the depth of the core, averaging −1.78‰ with a standard deviation of 0.64‰. The difference between bulk $\delta^{13}C$ and organic $\delta^{13}C$ oscillates between 0‰ and ~2‰ and tracks with carbonate abundance, indicating the isotopically heavier layers in the bulk mat $\delta^{13}C$ profile are in part due to the presence of carbonate.

To determine whether the mm-scale oscillations in the bulk mat $\delta^{13}C$ record can be explained by the activities of major primary producers within the photosynthetic mat,

© 2014 John Wiley & Sons Ltd

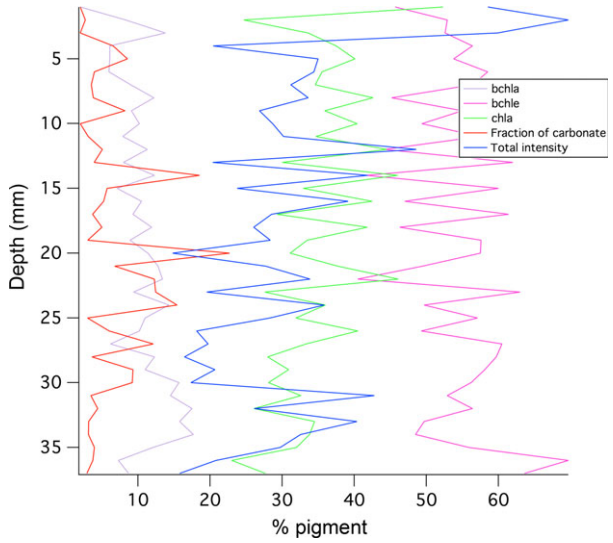

Fig. 5 Results of pigment analysis on core taken from Ames mat. Total intensity of all pigments together shows a marked decrease in pigment preservation at 4 mm below the mat surface, consistent with dense biomass in the surface of the mat. Superimposed on the plot is the fraction of $CaCO_3$ analyzed from this core, showing no significant correlation between pigment abundances and $CaCO_3$ abundance (r = 0.13 with chla; r = −0.14 with bchle).

pigment analysis was performed. Primary producers in these photosynthetic microbial mats have pigments that in some cases can be diagnostic for metabolic pathways (Table 1). For example, chlorophyll *a* (chla) is diagnostic for cyanobacteria, while bacteriochlorophyll *e* (bchle) is diagnostic for the green sulfur bacteria. Bacteriochlorophyll *a* (bchla) is shared by many phototrophs, but bacteriochlorophyll *b* (bchlb) is common only to purple sulfur and purple non-sulfur bacteria (Table 1). Concentrations of dominant pigments of the major primary producers were analyzed to characterize the relative abundances of the major photosynthetic groups (Fig. 5). Total intensity of the combined pigments decreases significantly below the top 3 mm, consistent with the texture of the mat, which is very dense in the top few mm.

Incubation experiments

We conducted a dual-labeled $^{13}C/^{15}N$ experiment to assess the potential uptake of DIC (HCO_3^-) and biomass production as a function of depth in the mat. Results of a 6-h incubation during peak sunlight indicate significant activity and biomass accumulation in the top 1–2 mm and moderate uptake of HCO_3^- and NH_4^+ in layers as deep as 19 and 8 mm, respectively (Fig. 6A,B). The top 3–4 mm is within the photic zone, and the stimulated activity is likely due to photosynthetic groups within the mat. Stimulation of HCO_3^- uptake deeper than 4 mm is likely from non-photosynthetic members of the mat such as colorless

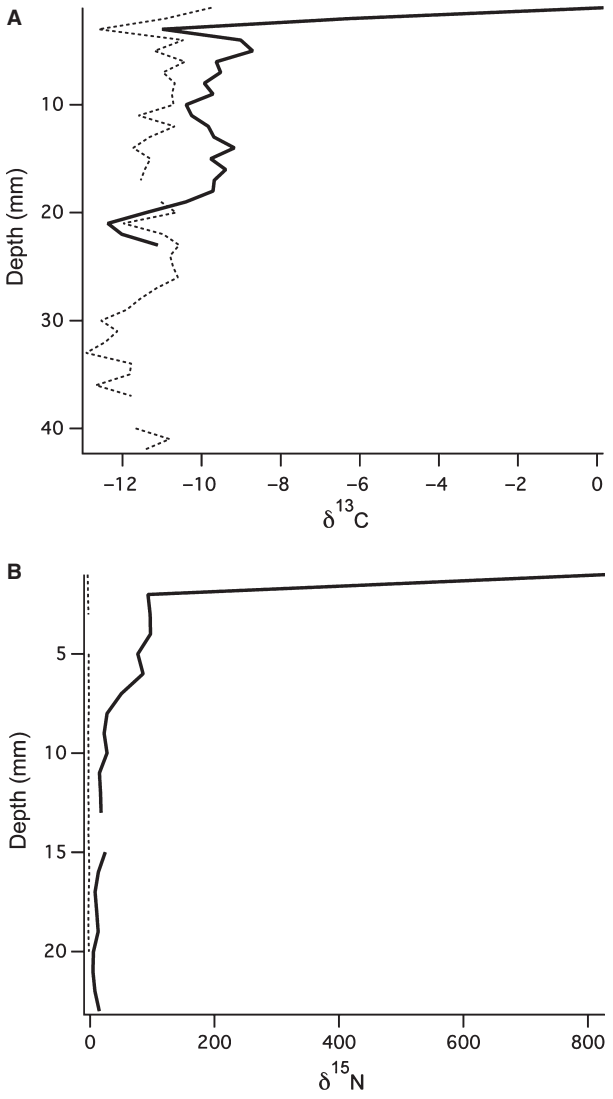

Fig. 6 Results of a 6-h incubation experiment (8:40 AM to 2:40 PM) with mat core submerged in flume water amended with ^{13}C-labeled HCO_3^- and ^{15}N-labeled NH_3. (A) Comparison of labeled mat (solid line) and unamended mat (dashed line) organic carbon $\delta^{13}C$ shows significantly greater uptake of labeled DIC in the top 2 mm compared to deeper in the mat, with virtually no label taken up deeper than 19 mm. (B) Comparison of labeled mat (solid line) and unamended mat (dashed line) organic matter $\delta^{15}N$ shows significant uptake in the top 1 mm and moderate uptake from 2 to 8 mm, indicating biomass accumulation.

sulfur bacteria (CSB) or autotrophic sulfate-reducing bacteria (SRB).

To determine where respiration is actively taking place in the mat, we conducted several incubation experiments with ^{13}C-labeled organic substrates to stimulate micro-organisms responsible for decomposition of mat, including SRB. Although these substrates likely stimulated growth of many types of heterotrophs, the combination of increased HS^- concentration at depth (determined with voltammetric profiles) and isotopic label uptake into the mat material

© 2014 John Wiley & Sons Ltd

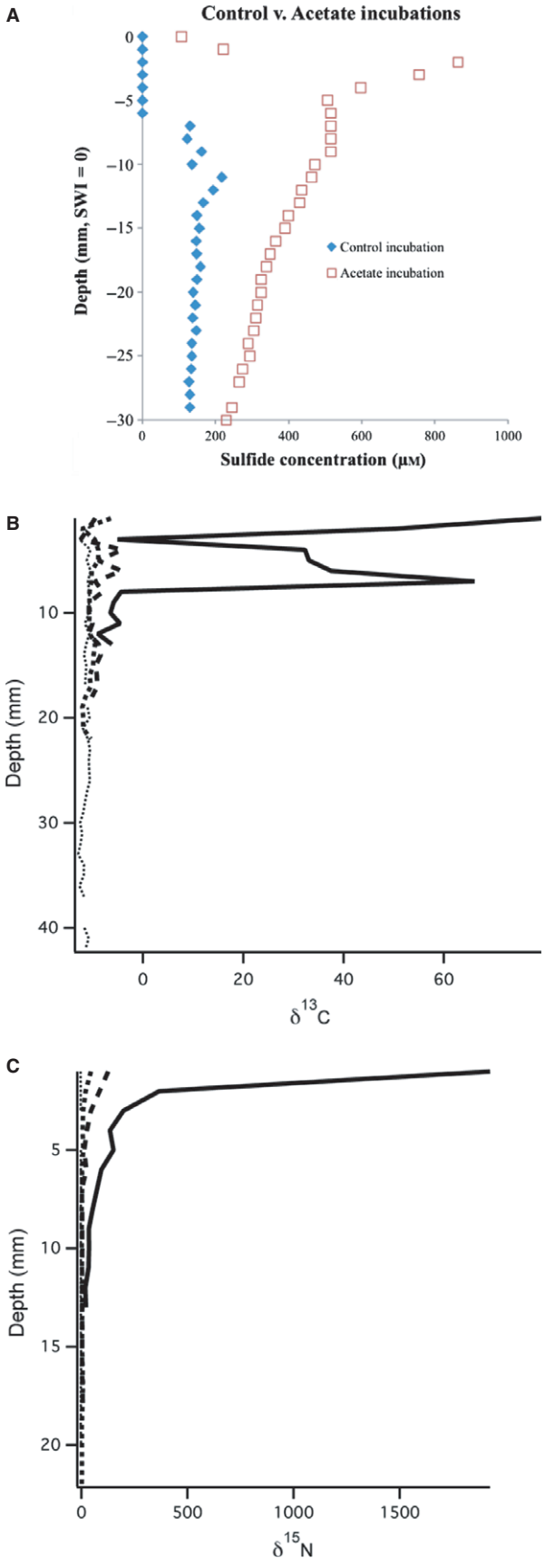

Fig. 7 Replicate mat pieces incubated under enrichment conditions under ambient light were removed and frozen for later isotopic analysis at 1 h (short dashed line), 2.75 h (long dashed line), and 6 h (dark solid line). (A) HS^- concentration profile after acetate enrichment compared to the control incubation. HS^- was elevated even up to the surface of the mat. (B) The acetate enrichment included additional ^{15}N-labeled NH_3. For reference, non-enriched mat (thin dotted line) $\delta^{15}N$ averages −2.2‰ to −0.6‰. (C) $\delta^{13}C$ profiles of time series enrichment experiments with ^{13}C-labeled acetate compared to the control mat.

highlights the layers with active bacterial sulfate reduction. Several substrates were tested, including methanol, acetate, bicarbonate, formate, and H_2 (g). Of those tested, only acetate enrichment produced a significant excess concentration of HS^- and incorporated large amounts of the ^{15}N and ^{13}C labels. The results of time series measurements (taken at 1, 2.75, and 6 h increments) during incubations with ^{13}C-labeled acetate and ^{15}N ammonium indicate gradual increase in the uptake of both ^{15}N-NH_3 and ^{13}C-acetate with time at all depths (Fig. 7). ^{13}C-acetate-derived carbon was incorporated mostly in the top 8 mm of mat, but modest incorporation occurred by micro-organisms residing in layers as deep as 18 mm (the base of the sampled mat material).

DISCUSSION

Carbon cycling: carbonate carbon and sulfate reduction

The ^{13}C-enriched values of biomass in the mat indicate CO_2 (aq) concentrations must be limiting, at least in the photic zone (Des Marais *et al.*, 1989; Bebout *et al.*, 2002). As such, the presence of carbonate in discrete layers within the mat coincident with CO_2 limitation can be understood as a result of *in situ* microbially mediated carbonate precipitation. We developed a carbonate speciation model incorporating diffusion, carbon fixation, and respiration to attempt to reconcile the apparent CO_2 limitation seen in the $\delta^{13}C$ of the mat with $S_2O_3^{2-}$ concentrations that result in calcite saturation. Respiration, fixation, and diffusion were allowed to modify the total DIC concentration (Fig. 8A,B), which was then respeciated using the pH profile obtained in this study (Fig. 8C). Respeciation assumes that the various DIC species have attained mutual chemical equilibrium, a process that can be slower than the biological CO_2 uptake rate, which cyanobacteria overcome using intracellular carbonic anhydrase that allows them to utilize bicarbonate (So & Espie, 2005). However, the model developed here does not try to distinguish this level of detail. The minimum in [DIC] occurred just below the surface of the mat, requiring a peak in fixation rate at 1 mm, consistent with results of Finke *et al.* (2013) who observed a peak in photosynthetic activity (both chla and bchla) at 1.3 mm depth. Further down, fixation rates

© 2014 John Wiley & Sons Ltd

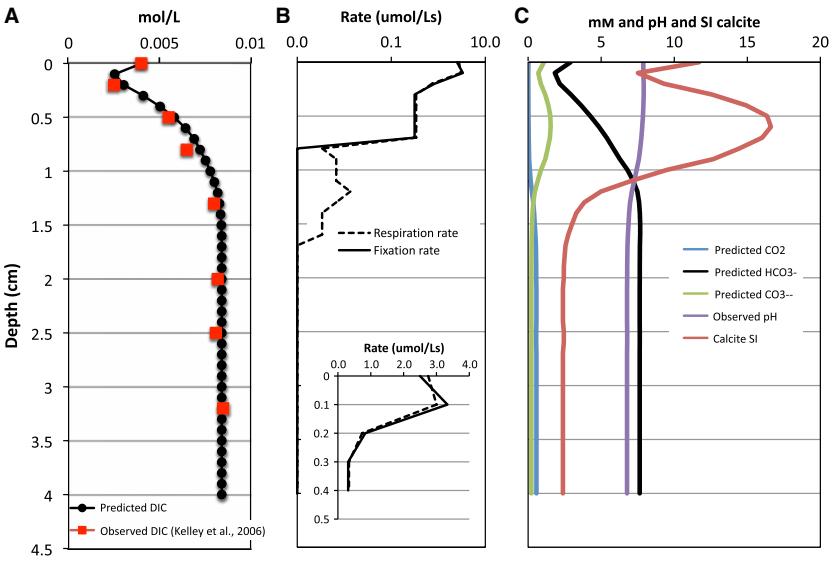

Fig. 8 Diffusional model showing the effect of respiration and carbon fixation on carbonate speciation based on observed pH profiles from this study, fitted to observations of DIC concentration reported in Kelley *et al.* (2006). (A) Predicted total DIC concentration with depth matches observed DIC. (B) Respiration and carbon fixation rates required to fit the DIC concentrations. Carbon fixation occurs down to 7 mm, with a roughly equal respiration rate, below which respiration exceeds fixation down to 17 mm. (C) Predicted carbonate speciation explains the scenario of limiting CO_2 above 10 mm simultaneous with calcite saturation (SI), primarily in the top 12 mm of the mat. [Ca++] is set at 25 mM.

decreased but were still greater than respiration, with a total carbon fixation rate from all photosynthetic processes decreasing from 3 to 0.3 μmol L^{-1} s^{-1} in the top 3 mm of mat (Fig. 8B). In these layers, carbon fixation draws down CO_2 (aq) such that HCO_3^- respeciates to provide additional CO_2 (aq). Between 3 and 7 mm, the respiration rate is constant but slightly higher than the fixation rate (Fig. 8B inset). The transition between carbon fixation and respiration at ~3 mm depth also corresponds to the phylogenetic stratigraphy reported in Harris *et al.* (2013). Below 7 mm, fixation drops to zero but the respiration rate increases slightly down to 17 mm. At these depths, the activity of SRB drops off (Canfield & Des Marais, 1993), suggesting respiration by other heterotrophs becomes important. Below 17 mm, minimal respiration must occur to maintain the observed constant [DIC]. The speciation of carbonate clearly indicates CO_2 limitation down to 12 mm depth, concurrent with a peak in [CO_3^-] and calcite saturation. Thus, it is possible to produce carbonate in layers in which primary carbon fixation is apparently CO_2 limited. The model also suggests that carbonate is primarily produced in the active upper layers of mat with a peak in saturation just below the photic zone. This suggests that carbonate found deeper in the mat is relict and retains the $\delta^{13}C$ signature of DIC in the overlying water column and uppermost mat layers. This is important because there is much discussion of potential alteration to $\delta^{13}C_{carb}$ signatures as the result of authigenic carbonate precipitation occurring within the sediments associated with a local DIC pool impacted by remineralization of organic carbon (e.g., Schrag *et al.*, 2013). In this case, despite the very high rates of microbial activity, there is little alteration to the $\delta^{13}C_{carb}$ signature observed in these mats. In addition, the correlation between abundance of GSB pigments and carbonate is evidence of a strong link between the SRB that produce conditions favorable for carbonate formation and GSB that utilize sulfide (Visscher *et al.*, 2010).

The change in respiration rate as a function of depth predicted by the model in Fig. 8B tracks with the change in uptake of ^{13}C-labeled acetate in the amendment experiment shown in Fig. 7 ($r^2 = 0.54$). Acetate enrichment stimulated sulfide production presumably by heterotrophic sulfate reducers capable of using acetate. This observation is consistent with the increase in sulfate-reducing populations previously observed by fluorescence in situ hybridization (FISH) within specific layers in the mat (~2, 8, and 10 mm) and previous observations of an increase in acetate-utilizing *Desulfobacter* sequences with depth in the mat (Fike *et al.*, 2009; Risatti *et al.*, 1994). The CO_2 produced by SRB grown on acetate has been shown to have $\delta^{13}C$ ~1‰ heavier than the substrate (Londry & Des Marais, 2003). The isotopic signature of carbonates (Fig. 4) varied between −0.84‰ and −3.1‰, with an average consistent with the expected value of −2.04‰ for HCO_3^- in equilibrium with CO_2 (g) at Baja (Keeling *et al.*, 2008). Therefore, the measured carbonate carbon isotopic values would have derived from DIC having a range in $\delta^{13}C$ from −4.9 to −2.6‰, consistent with the results of pore water $\delta^{13}C_{DIC}$ reported in Kelley *et al.* (2006). The activity of SRB will locally increase the concentration of CO_3^- that

© 2014 John Wiley & Sons Ltd

could cause precipitation of calcite within the mat (Figs 8C and 9), possibly incorporating an altered $\delta^{13}C_{DIC}$ signature as a result of respiration.

Isolating the cause of such a small isotopic shift between the expected $\delta^{13}C_{carb}$ derived from inorganic DIC in the overlying water column and the $\delta^{13}C_{carb}$ observed in the mat is difficult given the many possible causes. Possible processes that cause shifts in $\delta^{13}C_{carb}$ are reviewed in Sumner (2001) and include (1) recrystallization, (2) remineralization of isotopically light organic C resulting in more depleted $\delta^{13}C$ of pore water DIC during burial, (3) temperature change causing $\delta^{13}C_{carb}$ to increase at lower temperatures, and (4) rapid calcite precipitation rates causing depletions in $\delta^{13}C_{carb}$ due to disequilibrium effects. If we consider option (2), and assuming respiration by heterotrophic SRB using organic compounds derived from decomposing mat ($\delta^{13}C_{org}$ ~−11‰) results in $\delta^{13}C_{DIC}$ of −10‰ and that a simple weighted average of water column DIC and microbial DIC describes the resulting $\delta^{13}C_{carb}$ signal, then a contribution of 8–35% of DIC from heterotrophic SRB (or other respirers) could explain the $\delta^{13}C_{carb}$ we observe. However, we cannot rule out additional causes such as temperature shifts either between day/night conditions or between seasons, disequilibrium effects due to increased precipitation rates caused by high respiration rates, or carbonate recrystallization at depth within the mat.

The combined result is that (1) carbonates precipitating in the active top layers of these mats and subsequently buried exhibit only a slight shift in $\delta^{13}C_{carb}$ from the overlying water $\delta^{13}C_{DIC}$, *despite a high rate of microbial metabolic activity*, and (2) associated organic carbon that might become preserved in the rock record exhibits a strongly dampened biogenic fractionation. Other modern microbial mat systems that alternatively exhibit slower carbon fixation rates and/or have higher rates of sulfate reduction from autotrophic growth should exhibit a much greater effect on the $\delta^{13}C$ of *in situ* organic matter and carbonates, respectively. In addition, these results have implications for the interpretation of carbonate carbon isotope records through Earth history, as the increased activity of sulfate reducers would have resulted in increased saturation of carbonate with a larger signature of biogenic DIC, potentially shifting the $\delta^{13}C$ signature recorded in carbonates.

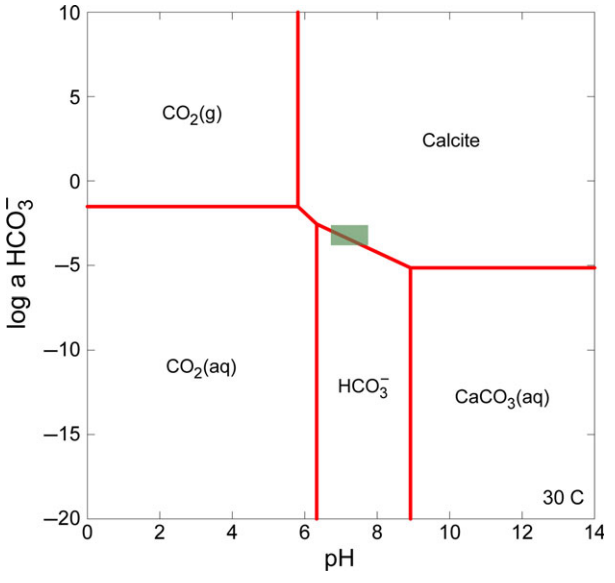

Fig. 9 Activity diagram of the CO_2–H_2O–Ca system at 30 °C and seawater activity of 0.025 for Ca^{++}. The pH monitored within the mat ranges between 7.9 near the surface and 6.8 at depth. Concentrations of DIC in these mats in situ were reported as ranging from 4 to 8 mM and in the Ames greenhouse mats from 2 to 4 mM (Kelley *et al.*, 2006) and are represented by the green box.

Carbon cycling: organic carbon

The $\delta^{13}C_{org}$ and $\delta^{13}C_{bulk}$ values observed correspond well with previous studies of the Guerrero Negro mats, despite their artificial environment in the flume at Ames (Des Marais *et al.*, 1989; Bebout *et al.*, 2002; Kelley *et al.*, 2006). The Guerrero Negro mats have a somewhat heavier carbon isotopic signature than other well-studied hypersaline microbial mats such as those at Solar Lake, Egypt (Schidlowski *et al.*, 1994) or Salin-de-Giraud, Camargue, France (Wieland *et al.*, 2008). This has been attributed to greater CO_2 (aq) limitation during mat formation leading to lower fractionations by the photosynthetic groups, mainly filamentous anoxygenic phototrophs (FAP) and cyanobacteria (Des Marais *et al.*, 1989; Wieland *et al.*, 2001; Ley *et al.*, 2006). It has been shown that competition between oxygenic phototrophs (CYA) and anoxygenic phototrophs (e.g., PSB) leads to CO_2 (aq) limitation sufficient to inhibit O_2 production by cyanobacteria, consistent with observed decreases in isotopic fractionation (Finke *et al.*, 2013).

We tested the use of pigment abundances as biomarkers indicative of carbon metabolism by building a simple model of carbon isotope fractionation for the Ames mat using equations (4) and (5). For each layer, the starting $\delta^{13}C$ value for CO_2 (aq) is determined using the equilibrium fractionation factor associated with the conversion of CO_2 (g) to CO_2 (aq) at 30 °C (−1.04‰; Mook *et al.*, 1974) and the reported value for atmospheric CO_2 (g) at the Baja station from December 2008 (Keeling *et al.*, 2008) of −8.35‰. This initial $\delta^{13}C$ of CO_2 (aq) is reduced by the Δ_{micr}, using the measured abundances and the published ranges of fractionation factors for each photosynthetic group in the mat (Table 1), to produce a predicted $\delta^{13}C_{org}$ value resulting from primary production. Equation (5) inherently assumes the pigment content to biomass ratio is comparable between the different clades. In fact, GSB at their highest metabolic rate contain about

© 2014 John Wiley & Sons Ltd

twice the amount of bchle per mg protein than either PSB or CYA (de Wit *et al.*, 1988; de Wit & van Gemerden, 1990; Overmann *et al.*, 1992). However, the metabolic rate of GSB under ideal conditions is about half that of CYA (de Wit *et al.*, 1988; Overmann *et al.*, 1992); thus, relative pigment abundance will approximate relative metabolic rates between different clades. Because this predication is based on standard fractionation factors for these metabolisms (Table 1), the result is isotopically light compared to the observed organic matter signature in these mats (Fig. 10).

Des Marais *et al.* (1989) suggested a mechanism that explains the heavier than expected $\delta^{13}C$ signatures commonly found in dense microbial mats as being a function of rapid carbon fixation rates in the mat. For the following, we assume that every layer of mat was originally formed at the surface. The uppermost 1 mm of mat is dominated by cyanobacterial oxygenic photosynthesis, the rate of which is maximized at high light levels (Fig. 11A). Such high carbon fixation rates (Fig. 11C) draw down the available CO_2 in the micro-environment surrounding the cells such that diffusion and respeciation of bicarbonate are insufficient to resupply CO_2 to the cells, resulting in decreased carbon isotopic fractionation (Des Marais, 1995). As growth of the mat causes successive layers to become buried, the carbon fixation rate of cyanobacteria slows due to light limitation (Fig. 11C) and activity of other phototrophs (GSB, PSB, PnonSB) with maximized activities at low light levels (Fig. 11B) becomes more prominent (Finke *et al.*, 2013). Light penetration within the *in situ* mats has been measured previously and for non-photosynthetically relevant wavelengths (e.g., 600 nm) penetrates at least as deep as 2.5 mm in the mat, while wavelengths used for photosynthesis (e.g., 450 and 670 nm) are more strongly attenuated (Jørgensen & Des Marais, 1988). For this study, we consider the top 3 mm to be within the photic zone. In our model, biomass in the top 1-mm layer is composed entirely of cyanobacteria growing with maximum activity rates in ideal light and carbon conditions, resulting in highest activity rates, carbon limitation, and subsequently a low f_{fix} of 0.2 (Fig. 12A,B). As cyanobacteria in deeper layers are subject to lower light levels and more limiting DIC concentrations as a result of scavenging in the upper layers, their rate of activity decreases gradually to zero at the base of the photic zone. As activity rate decreases, the instantaneous f_{fix} increases to 1.0 (i.e., maximum isotopic fractionation); the net f_{fix} is determined by the weighted sum of buried biomass produced under low f_{fix} and biomass produced at depth under higher f_{fix} (Fig. 12A). Thus, the net f_{fix} gradually increases to 0.4 in the top 3 mm (Fig. 12B), resulting in greater isotopic fractionation as the cyanobacterial CO_2 fixation rate decreases and becomes more comparable to the diffusion rate (Fig. 12A); thus, f_{fix} is effectively a fractionation dampening factor. The activity of GSB and PSB remains constant with a low net f_{fix} (0.1) below 1 mm depth due to carbon limitation as they are outcompeted by cyanobacteria in the upper layers, with their contribution to the total biomass determined by relative pigment abundances (Fig. 12B). The results of an amendment experiment using ^{13}C-labeled HCO_3^- (Fig. 6) and previous reports (Kelley *et al.*, 2006) support our model that assumes greater fixation rates in the top 2 mm. Results of this model are shown in Fig. 12B and match the top 3 mm of mat well, but show a $-1.5‰$ offset between 5 and 30 mm depth compared to the observed signature (Fig. 10, cross-hatching).

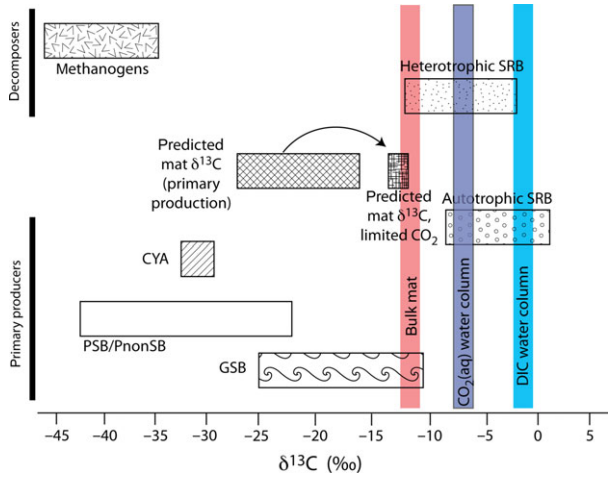

Fig. 10 Comparison of observed $\delta^{13}C$ of bulk mat and DIC sources with possible source microbial groups. The $\delta^{13}C$ of bulk mat based on the average of relative pigment abundances of photosynthetic primary producers (diamonds) is more depleted than the observations. Only a scenario in which a carbon fixation factor is applied that dampens the fractionation effect of primary producers (cross-hatching) predicts values near the observed range. Biomass of SRB using CO_2 or organic compounds from the mat is more enriched than the predicted and observed bulk mat. Methane produced from methanogenesis and subsequent biomass of methanotrophs are depleted relative to the bulk mat.

Decomposition processes that occur below the photic zone (e.g., fermentation, sulfate reduction, methanogenesis) subsequently alter the isotopic signature of biomass arising from primary production by Δ_{decomp}. Therefore, in our modified version of the model (equation 7), the $\delta^{13}C_{biomass}$ due to primary production determined by equation (5) using fractionation factors set to the maximum reported value (Table 1) is modified by a Δ_{decomp} resulting from superimposed processes such as sulfate reduction, fermentation, and methanogenesis that occur successively as the biomass is buried.

Changes in the *in situ* activity of sulfate-reducing bacteria (SRB) can be monitored by comparing changes in depth profiles of sulfide (HS^-) concentration within the mat. The observed sulfide concentrations represent minimum values for sulfide production given the simultaneous

© 2014 John Wiley & Sons Ltd

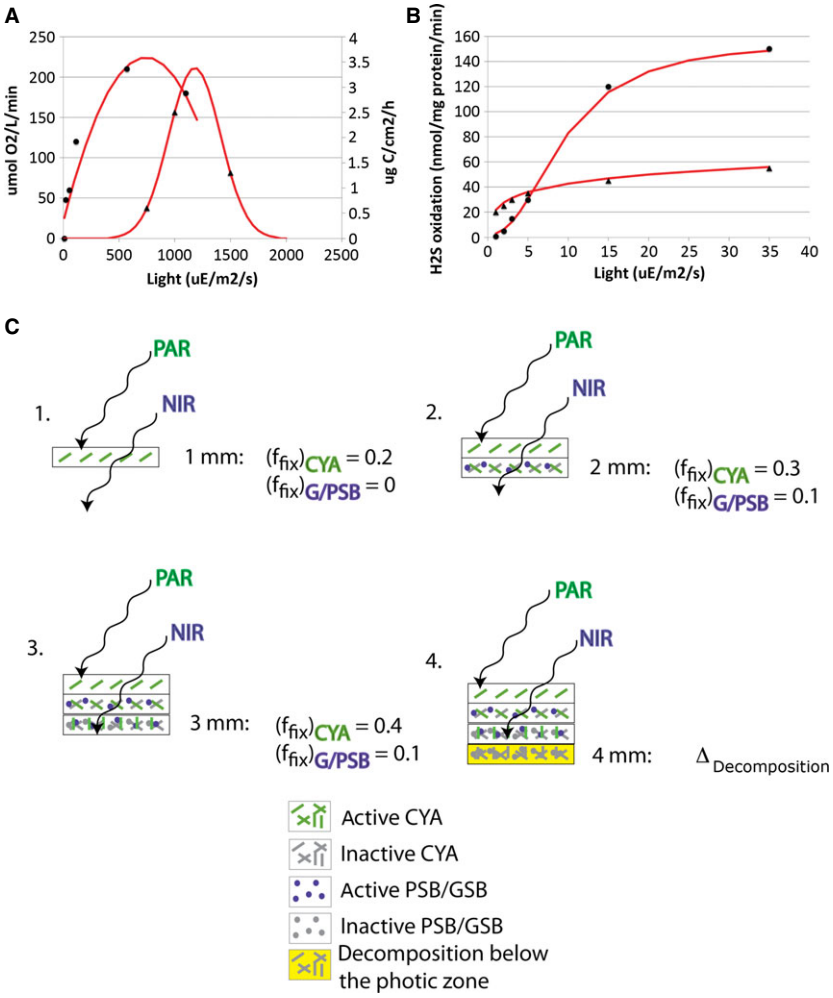

Fig. 11 (A) Photosynthetic activity of representative cyanobacteria as a function of light. Data for a *Halothece* strain (circles) are from Pringault and Garcia-Pichel (2000) and for a *Microcoleus* strain (triangles) are from Bebout *et al.* (1987). (B) Photosynthetic activity of representative purple sulfur bacteria as a function of light. Data for *Chlorobium* strain 2430 (circles) and strain MN1 (triangles) are from Overmann *et al.* (1992). (C) Schematic of microbial mat formation described by the model of equation (7). Mat is initially formed in (I) with the carbon fixation factors for cyanobacteria (CYA) and green and purple sulfur bacteria (G/PSB) as shown. As burial of old layers occurs with continued mat growth in (II) and (III), the net carbon fixation factors change as shown and include the inactive organic matter originally produced in the top 1 mm and the new organic matter produced consecutively at 2 and 3 mm. As near-infrared (NIR) energy penetrates deeper into the mat, G/PSB are stimulated down to the base of the photic zone at 3 mm depth. Below the photic zone, the inactive organic matter from photosynthetic activity will retain its isotopic signature from when it last was active (at 3 mm) and will become overprinted by decomposition processes as further burial takes place.

sulfide removal by sulfide oxidizers, both phototrophic and autotrophic. Amendment experiments with ^{13}C-labeled acetate stimulated sulfate reduction from the mat surface down to at least 15 mm (the deepest that was measured). A significant shift to lower uptake below 8 mm suggests a variable amount of microbial decomposition in the deeper portions of mat below the photic zone (Fig. 7). That acetate, of all substrates tested for SRB enrichment, stimulated the most activity is interesting given the results of Kelley *et al.* (2006), showing a stimulation of acetogens and acetate production within the greenhouse mats under low SO_4 conditions similar to those inferred for the Archean ocean (Canfield *et al.*, 2000; Habicht *et al.*, 2002). In addition, the dominant product of fermentation at night in these mats was found to be acetate, with up to 81% of electrons fixed during photosynthesis released as fermentation products at night (Lee *et al.*, 2014). Based on our sulfide profiles in the amendment experiments, we modified the model from Fig. 12B to include isotope fractionation resulting from decomposition, including sulfate reduction (Fig. 12C). At depths below 4 mm in the mat, the primary $\delta^{13}C$ signature is shifted and can be reproduced by decreasing the $\Delta_{overall}$ by incorporating a $-1‰$ Δ_{decomp}, consistent with secondary biomass production from decomposition of primary biomass (Abraham *et al.*, 1998; Hayes, 1993), a significant portion of which could be due to SRB utilizing the organic products of cyanobacterial fermentation of bulk mat biomass during the night (Lee *et al.*, 2014). The onset of major decomposition is associated with a change to less physically coherent mat textures below this depth. The presence of low concentrations of H_2 (aq) has been documented in these mats (Hoehler *et al.*, 2001; Burow *et al.*, 2014) that could potentially support an autotrophic population. However, we did not observe significant stimulation of H_2S production in the H_2 amendment experiment, suggesting the autotrophic SRB component is negligible in this mat, at least over the timescales investigated. In addition, an autotrophic community might be expected to increase the density and coherence of the mat, while a heterotrophic community would contribute to the deterioration of mat integrity, as was observed.

© 2014 John Wiley & Sons Ltd

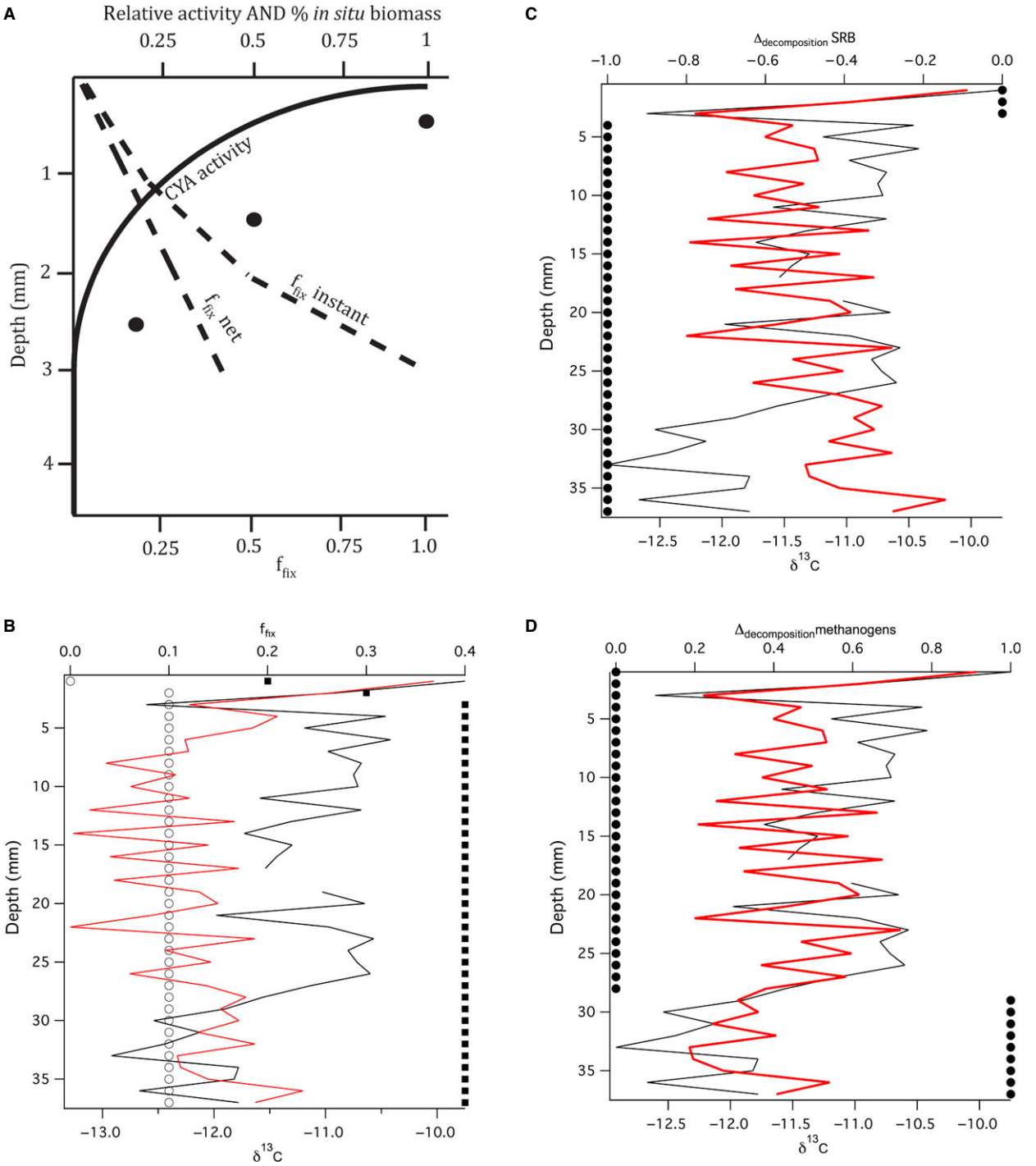

Fig. 12 Observed vs. modeled $\delta^{13}C$ in the mat. (A) The ratio f_{fix} for cyanobacteria is the carbon fixation factor. An f_{fix} value of 1 represents an unlimited fixation rate and results in maximum Δ_{micro}, while a value of zero would only occur at the highest carbon fixation rates such that microbes become isotopically non-selective and results in $\delta^{13}C_{org}$ identical to the CO_2 (aq) in the overlying water column (−7.31‰). As the activity and carbon availability change with depth in the mat, the instantaneous f_{fix} increases, but the contribution of buried biomass produced at the surface to each successive layer results in a net f_{fix} that is less. The values shown here are based on hypothetical values for % *in situ* biomass (circles) where the remaining fraction of biomass is buried material from the 1-mm layer above. (B) The modeled $\delta^{13}C$ of biomass assumes a $(f_{fix})_{CYA}$ shown in solid squares and a $(f_{fix})_{P/GSB}$ shown in open circles. The resulting predicted $\delta^{13}C_{org}$ of the mat is shown as a solid black line compared to the observed $\delta^{13}C_{org}$ shown as a gray line. (C) Comparison of observed $\delta^{13}C$ profile (gray line) and the model (dark solid line) that assumes an additional fractionation associated with decomposition (Δ_{decomp}) by SRB in the mat. (D) Comparison as in (C) with the addition of biomass contribution from methanogens at depth resulting in the final model profile (dark solid line). Changes in Δ_{decomp} with depth are discussed in the text.

© 2014 John Wiley & Sons Ltd

Below 27 mm, the $\delta^{13}C$ signature is again shifted, this time by $-1‰$ from the predicted decomposed signature. Several scenarios could possibly create the observed shift in $\delta^{13}C_{org}$ deeper in the mat. If the deep layers formed in the past were under less CO_2 (aq) limitation, then the original $\delta^{13}C_{org}$ value could have been correspondingly lower. This scenario seems unlikely, however, given that the water flow and evaporation rate in the hypersaline ponds at Guerrero Negro have been artificially controlled for the past 50 years. A second possibility that could explain the observed shift in $\delta^{13}C_{biomass}$ below 27 mm is that methylotrophic methanogens contribute to the organic carbon $\delta^{13}C$ at depth in the mat. Methanogens such as *Methanococcoides* previously observed in the Guerrero Negro mats (Summons *et al.*, 1998; Orphan *et al.*, 2008) preferentially utilize C1 compounds that could derive from decomposition products from the bulk mat biomass. Low concentrations of methane have been measured at depth in the mat (2–3 μM below 10 mm; Kelley *et al.*, 2006); together with metabolic gene surveys and lipid biomarker analyses indicating diverse methanogenic communities in these mats (Jahnke *et al.*, 2008; Orphan *et al.*, 2008), these data suggest methane cycling at depth within the mat. In addition, previous amendment experiments using trimethylamine substrate on Guerrero Negro mat resulted in enrichments of *Methanolobus and Methanohalophilus* within the mat and *Methanococcoides* in the sediments underlying the mat (Orphan *et al.*, 2008). The final model based on variable carbon fixation by primary producers as determined by relict pigment concentrations overprinted by biomass contributions from SRB and subsequently methanogens at the base of the mat reproduces the $\delta^{13}C$ of the organic matter reasonably well. These results suggest that the aggregate organic carbon isotope signature in these microbial mats is the result of complex primary and secondary microbial processes. In sediments, $\delta^{13}C_{org}$ integrates over activity in the water column, at the sediment–water interface, and deeper within sediments. These observations are critical for Earth history applications, where bulk $\delta^{13}C_{org}$ values are often used to infer biological fractionation from DIC and applied to reconstruct microbial ecology and metabolic activity, as well as the operation of the ancient carbon cycle.

CONCLUSIONS

Relative abundances of photosynthetic functional guilds that were assigned based on primary pigment analysis were used to predict the profile of $\delta^{13}C_{org}$ throughout the mat. Pigments are sufficiently well preserved even after partial decomposition to be useful bioindicators of primary productivity in mats, elucidating the variable contribution of functional groups to total mat biomass. In the photic zone of the mat, the rate of carbon fixation by cyanobacteria is highest in the top 1 mm, where isotopic fractionation during carbon fixation is lowest. Deeper in the photic zone, cyanobacterial growth slows down, increasing isotopic discrimination, concurrent with an increased biomass component from green and purple sulfur bacteria that is a function of relative abundance. Below the photic zone, small (~1‰) variations in the $\delta^{13}C_{org}$ composition are consistent with variable relative abundances of CYA (containing chla) and GSB (containing bchle), with CYA responsible for shifts to lighter $\delta^{13}C$ and GSB for heavier $\delta^{13}C$ in buried mat material. Overprinting this primary $\delta^{13}C$ signature in buried mat material is a process of secondary degradation of the mat contributing biomass first from SRB and other heterotrophs and at depths below 30 mm by additional methanogenic biomass. The combination of all these processes occurring in succession during burial is necessary to accurately explain the carbon isotope profile. From an Earth history perspective, paleoecological and paleoenvironmental studies using bulk $\delta^{13}C_{org}$ data need to take into account that these values represent the cumulative effects of microbial primary production and heterotrophic processing and as such may not necessary directly mirror primary water column activity.

Sulfate reduction was greatly stimulated by acetate enrichment and indicated significant activity in the top 8 mm of mat followed by moderate, and vertically variable, activity down to at least 20 mm below the mat surface. This depth varying activity is consistent with the spatial structure of $\delta^{34}S_{H2S}$ profiles and SRB distribution previously reported from these mats (Fike *et al.*, 2008, 2009). Thus, the cause of isotopic variability may be the complex distribution of SRB utilizing different substrates in different depth horizons. The activity of SRB is responsible for simultaneously increasing *in situ* DIC concentrations and increasing pH of pore waters, in some layers resulting in saturation with respect to carbonate. The percent of carbonate present varies greatly with individual layers in the mat, although the $\delta^{13}C$ of carbonate is fairly uniform down core. The offset between $\delta^{13}C_{org}$ and $\delta^{13}C_{bulk}$ due to the variable contribution of relatively ^{13}C-enriched carbonate is statistically correlated to layers with higher relict abundances of green sulfur bacteria. These observations suggest that both microbial activity of sulfate-reducing bacteria and other heterotrophs associated with green sulfur bacteria are significant for the precipitation of authigenic carbonates in the mat and that such precipitation is a primary feature formed in the basal layers of the photic zone. The presence or absence of carbonate may be dictated by microbial activity changing local environmental conditions to allow saturation of carbonate. In this case, microbial activity does not appear to significantly affect the $\delta^{13}C$ signature of the authigenic carbonate precipitated. These results may have implications for interpretations of $\delta^{13}C_{carb}$ records in deep time, particularly widespread negative excursions in the Neoproterozoic (e.g., Fike *et al.*, 2006;

© 2014 John Wiley & Sons Ltd

Grotzinger *et al.*, 2011; Swanson-Hysell *et al.*, 2010), where authigenic precipitation of ^{13}C-depleted carbonates within sediments has been suggested as a mechanism to generate unusually depleted $\delta^{13}C_{carb}$ signatures (Schrag *et al.*, 2013).

ACKNOWLEDGMENTS

We would like to thank NASA AMES NAI team, particularly Mike Kubo, Linda Jahnke, and Abigail Green-Saxena for discussion and assistance in the laboratory and field, and Exportadora del Sal, S. A. for access to the field site. Funding for this work was supported by NSF EAR-1124389 as well as a Packard Fellowship and a Hansewissenschaftskolleg Fellowship to D.A.F., NSF EAR-1123391 to V.J.O, and NSF EAR-1304352 and EAR-1261423 to G.D.

REFERENCES

Abraham W-R, Hesse C, Pelz O (1998) Ratios of carbon isotopes in microbial lipids as an indicator of substrate usage. *Applied and Environmental Microbiology* **64**, 4202–4209.

Bebout BM, Garcia-Pichel F (1995) UV B-induced vertical migrations of cyanobacteria in a microbial mat. *Applied and Environmental Microbiology* **61**, 4215–4222.

Bebout BM, Carpenter SP, Des Marais DJ, Discipulo M, Embaye T, Garcia-Pichel F, Hoehler TM, Hogan M, Jahnke LL, Keller RM, Miller SR, Prufert-Bebout LE, Raleigh C, Rothrock M, Turk K (2002) Long-term manipulations of intact microbial mat communities in a greenhouse collaboratory: simulating earth's present and past field environments. *Astrobiology* **2**, 383–402.

Bosak T, Newman DK (2005) Microbial kinetic controls on calcite morphology in supersaturated solutions. *Journal of Sedimentary Research* **75**, 190–199.

Brendel PJ, Luther GW III (1995) Development of a gold amalgam voltammetric microelectrode for the determination of dissolved Fe, Mn, O_2, and S(-II) in porewaters of marine and freshwater sediments. *Environmental Science and Technology*, **29**, 751–761.

Burow LC, Woebken D, Marshall IPG, Singer SW, Pett-Ridge J, Prufert-Bebout L, Spormann AM, Bebout BM, Weber PK, Hoehler TM (2014) Identification of *Desulfobacterales* as primary hydrogenotrophs in a complex microbial mat community. *Geobiology* **12**, 221–230.

Canfield DE, Des Marais DJ (1991) Aerobic sulfate reduction in microbial mats. *Science* **251**, 1471–1473.

Canfield DE, Des Marais DJ (1993) Biogeochemical cycles of carbon, sulfur, and free oxygen in a microbial mat. *Geochimica et Cosmochimica Acta* **57**, 3971–3984.

Canfield DE, Habicht KS, Thamdrup B (2000) The Archean sulfur cycle and the early history of atmospheric oxygen. *Science* **288**, 658–661.

Dahl C (2008) Inorganic sulfur compounds as electron donors in purple sulfur bacteria. *In Sulfur Metabolism in Phototrophic Organisms* (eds Hell R, Dahl C, Knaff D, Leustek T). Springer, Drodrecht, the Netherlands, pp. 289–317.

Dahl C, Hell R, Leustek T, Knaff D (2008) Introduction to sulfur metabolism in phototrophic organisms. *In Sulfur Metabolism in Phototrophic Organisms* (eds Hell R, Dahl C, Knaff D, Leustek T). Springer, Drodrecht, the Netherlands, pp. 1–14.

Des Marais DJ (1995) The biogeochemistry of hypersaline microbial mats. *Advances in Microbial Ecology* **14**, 251–274.

Des Marais DJ, Cohen Y, Nguyen H, Cheatham M, Cheatham T, Munoz E (1989) Carbon isotopic trends in the hypersaline ponds and microbial mats at Guerrero Negro, Baja California Sur, Mexico: implications for Precambrian stromatolites. *In Microbial Mats: Physiological Ecology of Benthic Microbial Communities* (eds Cohen Y, Rosenberg E). Amer. Soc. Microbiology, Washington, DC, pp. 191–203.

Des Marais DJ, Strauss H, Summons RE, Hayes JM (1992) Carbon isotope evidence for the stepwise oxidation of the Proterozoic environment. *Nature* **359**, 605–609.

Dillon JG, Miller S, Bebout B, Hullar M, Pinel N, Stahl DA (2009) Spatial and temporal variability in a stratified hypersaline microbial mat community. *FEMS Microbiology Ecology* **68**, 46–58.

Dupraz C, Visscher PT (2005) Microbial lithification in marine stromatolites and hypersaline mats. *Trends in Microbiology* **13**, 429–438.

Emrich K, Ehhalt DH, Vogel JC (1970) Carbon isotope fractionation during the precipitation of calcium carbonate. *Earth and Planetary Science Letters* **8**, 363–371.

Farmer JD, Des Marais DJ (1994) Biological versus inorganic processes in stromatolite morphogenesis: Observations from mineralizing sedimentary systems. *Microbial Mats, NATO ASI Series* **35**, 61–68.

Fike DA, Grotzinger JP, Pratt LM, Summons RE (2006) Oxidation of the Ediacaran Ocean. *Nature* **444**, 744–747.

Fike DA, Gammon CL, Ziebis W, Orphan VJ (2008) Micron-scale mapping of sulfur cycling across the oxycline of a cyanobacterial mat: a paired nanoSIMS and CARD-FISH approach. *The ISME Journal* **2**, 749–759.

Fike DA, Finke N, Zha J, Blake G, Hoehler TM, Orphan VJ (2009) The effect of sulfate concentration on (sub)millimeter-scale sulfide $\delta^{34}S$ in hypersaline cyanobacterial mats over the diurnal cycle. *Geochimica et Cosmochimica Acta* **73**, 6187–6204.

Finke N, Hoehler TM, Polerecky L, Buehring B, Thamdrup B (2013) Competition for inorganic carbon between oxygenic and anoxygenic phototrophs in a hypersaline microbial mat, Guerrero Negro, Mexico. *Environmental Microbiology* **15**, 1532–1550.

Frigaard N-U, Larsen KL, Cox RP (1996) Spectrochromatogaphy of photosynthetic pigments as a fingerprinting technique for microbial phototrophs. *FEMS Microbiology Ecology* **20**, 69–77.

Frund C, Cohen Y (1992) Diurnal cycles of sulfate reduction under oxic conditions in cyanobacterial mats. *Applied and Environmental Microbiology* **58**, 70–77.

Garcia-Pichel F, Mechling M, Castenholz RW (1994) Diel migrations of microorganisms within a benthic, hypersaline mat community. *Applied and Environmental Microbiology* **60**, 1500–1511.

Grotzinger JP, Knoll AH (1999) Stromatolites in Precambrian carbonates: evolutionary mileposts or environmental dipsticks? *Annual Review of Earth and Planetary Sciences* **27**, 313–358.

Grotzinger JP, Fike DA, Fischer WW (2011) Enigmatic origin of the largest-known carbon isotope excursion in Earth's history. *Nature Geoscience* **4**, 285–292.

Habicht KS, Gade M, Thamdrup B, Berg P, Canfield DE (2002) Calibration of sulfate levels in the Archean ocean. *Science* **298**, 2372–2374.

© 2014 John Wiley & Sons Ltd

Harris JK, Caporaso JG, Walker JJ, Spear JR, Gold NJ, Robertson CE, Hugenholtz P, Goodrich J, McDonald D, Knights D, Marshall P, Tufo H, Knight R, Pace NR (2013) Phylogenetic stratigraphy in the Guerrero Negro hypersaline microbial mat. *The ISME Journal* **7**, 50–60.

Hayes JM (1993) Factors controlling ^{13}C contents of sedimentary organic compounds: principles and evidence. *Marine Geology* **113**, 111–125.

Hayes JM (2001) Fractionation of carbon and hydrogen isotopes in biosynthetic processes. *Reviews in Mineralogy and Geochemistry* **43**, 225–277.

Hoehler TM, Bebout BM, Des Marais DJ (2001) The role of microbial mats in the production of reduced gases on the early Earth. *Nature* **412**, 324–327.

Holland HD, Kuo PH, Rye RO (1994) O_2 and CO_2 in the late Archaean and early Proterozoic atmosphere. *Mineralogical Magazine* **58**, 424–425.

Jahnke LL, Orphan VJ, Embaye T, Turk KA, Kubo MD, Summons RE, Des Marais DJ (2008) Lipid biomarker and phylogenetic analyses to reveal archaeal biodiversity and distribution in hypersaline microbial mat and underlying sediment. *Geobiology* **6**, 394–410.

Jorgensen BB, Des Marais DJ (1986a) Competition for sulfide among colorless and purple sulfur bacteria in cyanobacterial mats. *FEMS Microbiology Ecology* **38**, 179–186.

Jorgensen BB, Des Marais DJ (1986b) A simple fiber-optic microprobe for high resolution light measurements: application in marine sediment. *Limnology and Oceanography* **31**, 1376–1383.

Jørgensen BB, Des Marais DJ (1988) Optical properties of benthic photosynthetic communities: fiber-optic studies of cyanobacterial mats. *Limnology and Oceanography* **33**, 99–113.

Jørgensen BB, Revsbech NP, Blackburn TH, Cohen Y (1979) Diurnal cycle of oxygen and sulfide microgradients and microbial photosynthesis in a cyanobacterial mat sediment. *Applied and Environmental Microbiology* **38**, 46–58.

Keeling RF, Piper SC, Bollenbacher AF, Walker JS (2008) Atmospheric CO_2 records from sites in the SIO air sampling network. *In Trends: A Compendium of Data on Global Change*. Carbon Dioxide Information Analysis Center, Oak Ridge National Laboratory, U.S. Department of Energy, Oak Ridge, TN.

Kelley CA, Prufert-Bebout LE, Bebout BM (2006) Changes in carbon cycling ascertained by stable isotopic analyses in a hypersaline microbial mat. *Journal of Geophysical Research: Biogeosciences* **111**, G04012.

Kuhl M, Fenchel T, Kazmierczak J (2003) Growth, structure and calcification potential of an artificial cyanobacterial mat. In *Fossil and Recent Biofilms, A Natural History of Life on Planet Earth* (eds Krumbein WE, Paterson D, Zavarzin G). Kluwer Academic Publishers, Drodrecht, the Netherlands, pp. 77–102.

Kump LR, Arthur MA (1999) Interpreting carbon-isotope excursions: carbonates and organic matter. *Chemical Geology* **161**, 181–198.

Lee JZ, Burow LC, Woebken D, Everroad RC, Kubo MD, Spormann AM, Weber PK, Pett-Ridge J, Bebout BM, Hoehler TM (2014) Fermentation couples Chloroflexi and sulfate-reducing bacteria to Cyanobacteria in hypersaline microbial mats. *Frontiers in Microbiology* **5**, 1–17.

Ley RE, Harris JK, Wilcox J, Spear JR, Miller SR, Bebout BM, Maresca JA, Bryant DA, Sogin ML, Pace NR (2006) Unexpected diversity and complexity of the guerrero negro hypersaline microbial mat. *Applied and Environmental Microbiology* **72**, 3685–3695.

Londry KL, Des Marais DJ (2003) Stable carbon isotope fractionation by sulfate-reducing bacteria. *Applied and Environmental Microbiology* **69**, 2942–2949.

Meites L, Delahay P (1966) Polarographic techniques. *Journal of the Electrochemical Society*, **113**, 124C–124C.

Millero FJ (1995) Thermodynamics of the carbon dioxide system in the oceans. *Geochimica et Cosmochimica Acta* **59**, 661–677.

Millero FJ, Pierrot D, Lee K, Wanninkhof R, Feely R, Sabine CL, Key RM, Takahashi T (2002) Dissociation constants for carbonic acid determined from field measurements. *Deep-Sea Research Part I: Oceanographic Research Papers* **49**, 1705–1723.

Minz D, Flax JL, Green SJ, Muyzer G, Cohen Y, Wagner M, Rittmann BE, Stahl DA (1999) Diversity of sulfate-reducing bacteria in oxic and anoxic regions of a microbial mat characterized by comparative analysis of dissimilatory sulfite reductase genes. *Applied and Environmental Microbiology* **65**, 4666–4671.

Mook WG, Bommerson JC, Staverman WH (1974) Carbon isotope fractionation between dissolved bicarbonate and gaseous carbon dioxide. *Earth and Planetary Science Letters* **22**, 169–176.

Orphan VJ, Hinrichs KU, Ussler W III, Paull CK, Taylor LT, Sylva SP, Hayes JM, DeLong EF (2001) Comparative analysis of methane-oxidizing archaea and sulfate-reducing bacteria in anoxic marine sediments. *Applied and Environmental Microbiology* **67**, 1922–1934.

Orphan VJ, Orphan LL, Embaye T, Turk KA, Pernthaler A, Summons RE, Des Marais DJ (2008) Characterization and spatial distribution of methanogens and methanogenic biosignatures in hypersaline microbial mats of Baja California. *Geobiology* **6**, 376–393.

Overmann J, Cypionka H, Pfennig N (1992) An extremely low-light-adapted phototrophic sulfur bacterium from the Black Sea. *Limnology and Oceanography* **37**, 150–155.

Pringault O, Garcia-Pichel F (2000) Monitoring of oxygenic and anoxygenic photosynthesis in a unicyanobacterial biofilm, grown in benthic gradient chamber. *FEMS Microbiology Ecology*, **33**, 251–258.

Riding R (2000) Microbial carbonates: the geological record of calcified bacterial–algal mats and biofilms. *Sedimentology* **47**, 179–214.

Risatti JB, Capman WC, Stahl DA (1994) Community structure of a microbial mat: the phylogenetic dimension. *Proceedings of the National Academy of Sciences* **91**, 10173–10177.

Saltzman MR, Thomas E (2012) Carbon isotope stratigraphy. *In The Geologic Time Scale 2012* (eds Gradstein F, Ogg J, Ogg G, Schmitz M). Elsevier, Waltham, MA, pp. 207–232.

Sander J, Dahl C (2008) Metabolism of inorganic sulfur compounds in purple bacteria. *In The Purple Phototrophic Bacteria* (eds Hunter CN, Daldal F, Thurnauer MC, Beatty JT). Springer, London, pp. 595–622.

Schidlowski M, Gorzawski H, Dor I (1994) Carbon isotope variations in a solar pond microbial mat: role of environmental gradients as steering variables. *Geochimica et Cosmochimica Acta* **58**, 2289–2298.

Schrag DP, Higgins JA, Macdonald FA, Johnston DT (2013) Authigenic carbonate and the history of the global carbon cycle. *Science* **339**, 540–543.

Slowey AJ, DiPasquale MM (2012) How to overcome inter-electrode variability and instability to quantify dissolved oxygen, Fe(II), Mn(II), S(-II) in undisturbed soils and sediments using voltammetry. *Geochemical Transactions* **13**, 6.

© 2014 John Wiley & Sons Ltd

So AKC, Espie GS (2005) Cyanobacterial carbonic anhydrases. *Canadian Journal of Botany* **83**, 721–734.
Summons RE, Franzmann PD, Nichols PD (1998) Carbon isotopic fractionation associated with methylotrophic methanogenesis. *Organic Geochemistry* **28**, 465–475.
Sumner DY (2001) Microbial influences on local carbon isotopic ratios and their preservation in carbonate. *Astrobiology* **1**, 57–70.
Swanson-Hysell NL, Rose CV, Calmet CC, Halverson GP, Hurtgen MT, Maloof AC (2010) Cryogenian glaciation and the onset of carbon-isotope decoupling. *Science* **328**, 608–611.
Swart PK (2008) Global synchronous changes in the carbon isotopic composition of carbonate sediments unrelated to changes in the global carbon cycle. *Proceedings of the National Academy of Sciences, USA* **37**, 13741–13745.
Teske A, Ramsing NB, Habicht K, Fukui M, Kuver J, Jorgensen BB, Cohen Y (1998) Sulfate-reducing bacteria and their activities in cyanobacterial mats of Solar Lake (Sinai, Egypt). *Applied and Environmental Microbiology* **64**, 2943–2951.
Visscher PT, Dupraz C, Braissant O, Gallagher KL, Glunk C, Casillas L, Reed RES (2010) Biogeochemistry of carbon cycling in hypersaline mats: linking the present to the past through biosignatures. *Microbial Mats: Cellular Origin, Life in Extreme Habitats and Astrobiology* **14**, 443–468.
Webb SM (2005) SIXPack: a Graphical User Interface for XAS Analysis Using IFEFFIT. *Physica Scripta* **T115**, 1011–1014.
Wieland A, de Beer D, Damgaard LR, Kuhl M, van Dusschoten D, Van As H (2001) Fine-scale measurement of diffusivity in a microbial mat with nuclear magnetic resonance imaging. *Limnology and Oceanography* **46**, 248–259.
Wieland A, Pape T, Mobius J, Klock J-H, Michaelis W (2008) Carbon pools and isotopic trends in a hypersaline cyanobacterial mat. *Geobiology* **6**, 171–186.
de Wit R, Boekel WHM, van Gemerden H (1988) Growth of the cyanobacterium Microcoleus chtonoplastes on sulfide. *FEMS Microbiology Ecology*, **53**, 203–209.
de Wit R, van Gemerden H (1990) Growth of the phototrophic purple sulfur bacterium *Thiocapsa roseopersicina* under oxic/anoxic regimens in the light. *FEMS Microbiology Ecology* **73**, 69–76.
Wong W, Sackett WM, Benedict CR (1975) Isotope fractionation in photosynthetic bacteria during carbon dioxide assimilation. *Plant Physiology* **55**, 475–479.
Zyakun AM, Lunina ON, Prusakova TS, Pimenov NV, Ivanov MV (2009) Fractionation of stable carbon isotopes by photoautotrophically growing anoxygenic purple and green sulfur bacteria. *Microbiology* **78**, 757–768.

© 2014 John Wiley & Sons Ltd